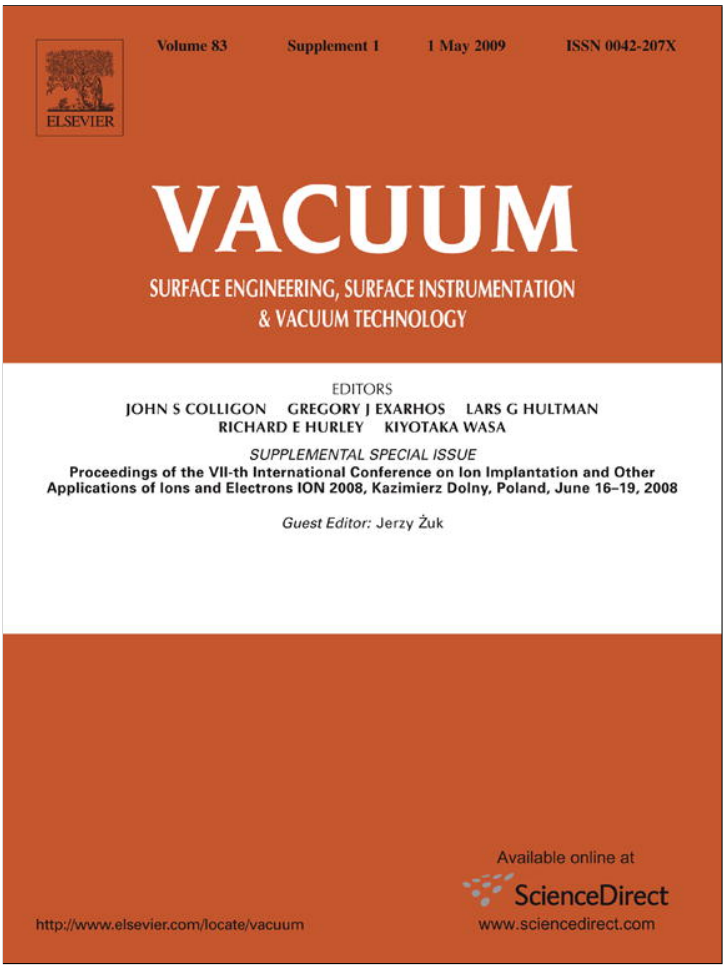

Vacuum 83 (2009) S240–S244

Contents lists available at ScienceDirect

Vacuum

journal homepage: www.elsevier.com/locate/vacuum

Structures and properties of Ti alloys after double implantation

A.D. Pogrebnjak [a,e,*], S.N. Bratushka [a,e], V.V. Uglov [c], V.S. Rusakov [b], V.M. Beresnev [a,e], V.M. Anischik [c], L.V. Malikov [a,e], N. Levintant [f], P. Zukovski [d]

[a] Sumy Institute for Surface Modification, P.O. Box 163, 40030 Sumy, Ukraine
[b] Moscow State University, Moscow, Russia
[c] Belarus State University, Minsk, Belarus
[d] Lublin Technical University, Lublin, Poland
[e] G.V. Kurdyumov Institute of Metal Physics NAS of Ukraine
[f] Institute of Fundamental Technological Research, Warsaw, Poland

ARTICLE INFO

Article history:
Received 16 June 2008
Received in revised form
29 January 2009
Accepted 30 January 2009

Keywords:
Implantation
Structure
Ti alloys
Composition
Hardness

ABSTRACT

The paper presents new results on investigation of structure and physical-mechanical properties of near surface layers of titanium alloys after (W^+, Mo^+) ion implantation and subsequent thermal annealing under 550 °C for 2 h. Using back scattering (RBS) of helium ions and protons, scanning electron microscopy (SEM) with microanalysis (EDS), (WDS), proton (ion) induced X-ray emission (PIXE), X-ray phase analysis (XRD) with a grazing incidence geometry (0.5° angle), measurements of nanohardness and elastic modulus, friction wear (cylinder-plate), measurements of corrosion resistance in a salt solution, we investigated the VT-6 samples, and determined their fatigue resistance under cyclic loads. Double increase of hardness, decrease of wear and increased fatigue resistance were found, which was related to the formation of small dispersion (nanodimension) nitride, carbonitride, and intermetalloid phases.

1. Introduction

As it is known [1,2], transition of medium energy ions through a solid is accompanied by scattering at matrix atoms and electrons, which results in deceleration and changing of ion motion direction, shifting of crystal atoms from lattice sites, accumulation of impurities in a target, sputtering of material surfaces, atomic mixing, formation of distribution profiles of implanted ions, formation of new phases. This essentially influences their mechanical and chemical properties [1–4].

Application of high-fluence and intensive implantation results in shifting of an implanted ion concentration profile in the surface vicinity, due to enhancement of sputtering process [3,4]. We understand high-fluence and intensive ion implantation (HDIII) as an implantation under which the rate of fluence accumulation is about 10^{16} cm^2/min, concentration of implanted ions is from tens to 100 atomic per cent [5–9], and an ion current density in the target is from units to tens of milliamps under current pulse duration 100–200 μs.

Paper [4,5] demonstrated that double implantation of Cu^+, N^+ and Fe^+, Zr^+ into titanium alloys resulted in a change in microhardness, which was, first of all, related to surface layer hardening due to formation of martensite phases, small dispersion carbides and oxycarbides. In papers [5–8] it was found almost 80% increase of fatigue resistance in comparison with the initial samples under Hf ion implantation into titanium alloys [6,7]. In the mid-90s, it was demonstrated that C, N, B implantation increased a cyclic life of Ti-6% Al-4% (VT-6) alloy 4–5 times due to deceleration of dislocation motion and a decrease in fracture growth [6,10–12]. Also it is known that W and Mo can be applied as doping elements to increase hardness and improve servicing characteristics of construction materials [10–15].

In this connection, investigations of high-fluence and intensive W^+ and Mo^+ ion implantation (HDIII) effects on changes in physical–chemical and mechanical characteristics of titanium alloys VT-6 were of an undoubted interest.

2. Methods of sample preparation and investigations

The samples of VT-6 (Ti, Al ~ 5.5–6.8%, V ~ 3.5–4.5% of the mass content), of 15 × 15 × 2 dimensions, polished and annealed to reject residual stresses and cold working, were investigated. Metal ion implantation was performed in the vacuum-arc implantor "DIANA"

* Corresponding author. Sumy Institute for Surface Modification, P.O. Box 163, 40030 Sumy, Ukraine. Tel.: +380 542 78 39 86; fax: +380 542 78 89 10
E-mail address: apogrebnjak@simp.sumy.ua (A.D. Pogrebnjak).

0042-207X/$ – see front matter © 2009 Published by Elsevier Ltd.
doi:10.1016/j.vacuum.2009.01.072

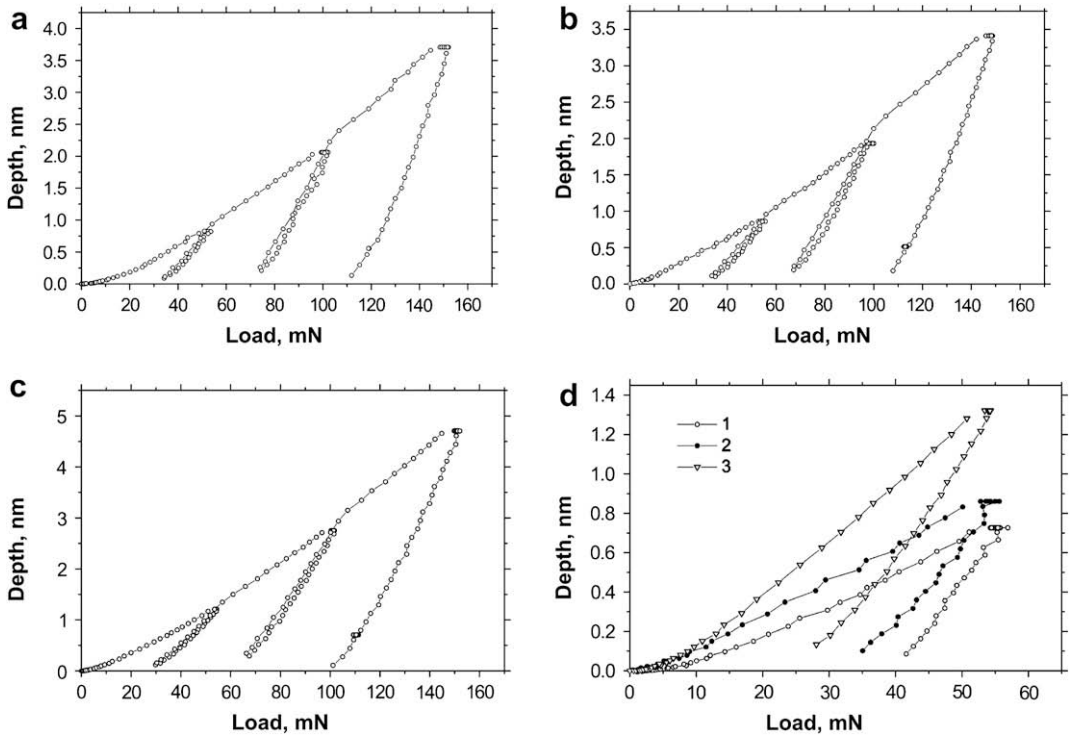

Fig. 1. A diagram of indentation penetration for an initial sample (a), after the implantation (b), after the annealing (c). The first loading cycle to 50 nm depth (d): 1 – for an initial sample, 2 – after the implantation, 3 – the annealing after the implantation.

under 5×10^{17} cm^{-2} fluence, 200 μs pulse duration, the sample surface temperature exceeded 300 °C. Ion implantation was performed in the accelerator chamber under 10^3 Pa residual vacuum.

To analyze the element composition of samples we applied the RBS method for helium ions of 2.035 MeV. The structure and surface relief analyses were performed with the aid of a scanning electron microscope REMMA with a microanalyzer WDS (Selmi, Sumy). To investigate the structure of titanium alloys VT-6, we applied a sliding beam in the Wulf–Bregg geometry, additionally we performed investigations of nanohardness and microhardness, wear resistance under friction of a cylinder over sample surfaces and measured fatigue resistance under cyclic loads (for some series of samples), using especially prepared samples looking like small dumb-bells.

The tests were performed using a three-face Berkovich indentation with a nanohardness measuring device Nano Indenter-II, MTS Systems Corp., Oak Ridge, TN, USA. In the process of testing with a high accuracy a dependence of the indenter top displacement on a load was registered. An accuracy of the print depth measurement was equal to ±0.04 nm, that of the indenter load ±75 nH. The device is able to perform about 3 load and displacement measurements per minute. To decrease vibrations the device was positioned at a vibration isolating table. In every test the indenter was loaded/unloaded three times, each time reaching higher load, which did not exceed 5 mH (≈0.5 G) with 150 nm depth.

After testing the hardness was measured according to the indentation print depth, and the elastic modulus was calculated by the unloading curve analysis [13–15].

3. Results and discussion

The hardness H and the elastic modulus E were determined using a nanohardness measuring device (Nan Indentor-II) according to the Oliver–Pharr [15] and Berkovich indentation methods. A value of elastic recovery W_e of a surface layer was calculated using the curves "loading–unloading" according to the formula:

$$W_e = \frac{h_{\max} - h_r}{h_{\max}}, \quad (1)$$

where $h_{\max}$ is a maximum indentor penetration depth, h_r is a residual depth after load relax.

The penetration diagrams are shown in Fig. 1a–d. A peculiarity of given diagrams is essentially high for a metal elastic recovery in indentor unloading. This indicates a low modulus of E elasticity with a relatively high hardness H (a value of the elastic recovery was determined by the ratio E/H). A load which was necessary for indentor penetration to 50 nm depth was minimum for an initial sample (0.8 ± 0.1 mH), increased to (0.9 ± 0.1 mH) for an implanted sample and was maximum for an implanted sample after annealing

Table 1
Results of hardness for VT-6, GPa.

Cast	Depth		
	50 nm	100 nm	150 nm
Before	5.8 ± 0.9	5.6 ± 0.8	5.0 ± 0.5
After implantation	6.8 ± 0.3	5.9 ± 0.4	5.2 ± 0.5
After annealing	10.7 ± 1.4	9.7 ± 0.8	8.5 ± 0.6

Table 2
Elastic modulus for VT-6, GPa.

Cast	Depth		
	50 nm	100 nm	150 nm
Before	123 ± 14	124 ± 21	141 ± 10
After implantation	127 ± 5	120 ± 5	115 ± 8
After annealing	164 ± 25	145 ± 9	140 ± 7

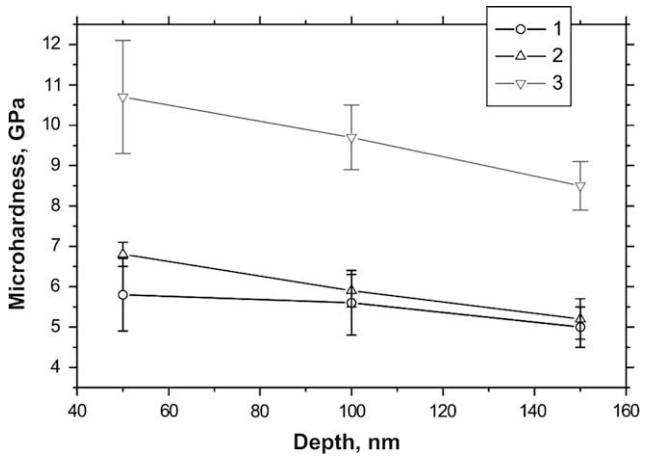

Fig. 2. Hardness vs depth: 1 – for an initial sample, 2 – the implantation, 3 – the annealing after the implantation.

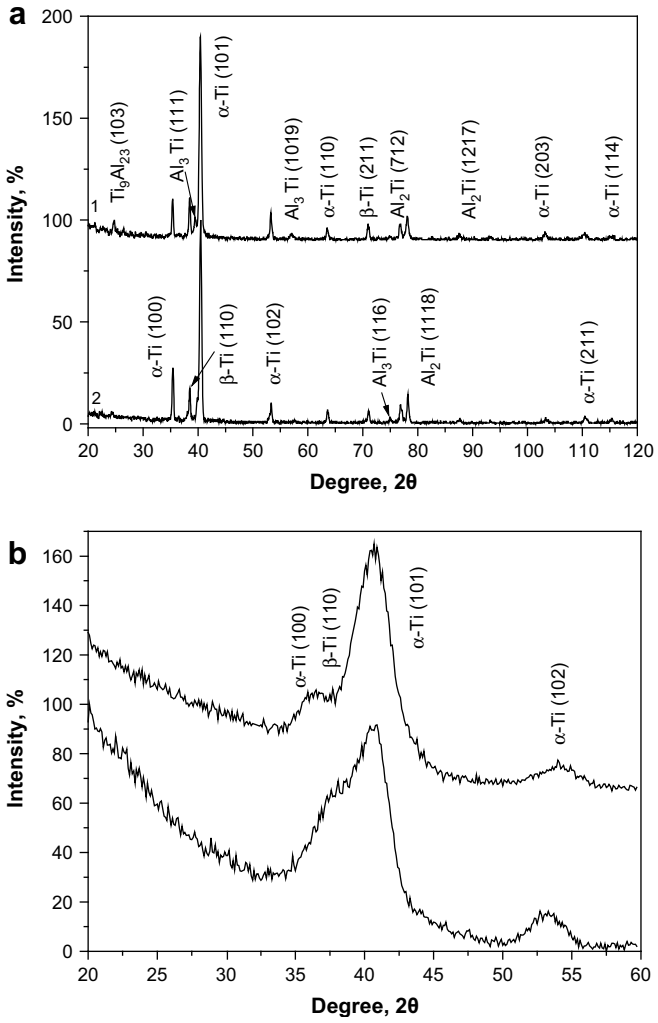

Fig. 3. Diffraction patterns obtained for the VT-6 samples a) after W and Mo ion implantation with 5×10^{17} cm^{-2} fluence, 60 keV (an upper curve) and after annealing at 550 °C for two hours (a lower curve). b) Measured in a grazing incident geometry at 0.5° slope angle in the regions (100) and (101) α-Ti, and additional line (111) Al_3Ti. An upper curve was taken after W and Mo ion implantation with 5×10^{17} cm^{-2} fluence. A lower curve was taken after annealing at 550 °C for 2 h.

$(1.2 \pm 0.1$ mH). This indicates growing hardness of the surface layer after implantation and annealing.

The fact that an elastic recovery of a print depth in unloading after annealing was much longer than that for an initial one is worth our attention. This indicates that hardness growth was accompanied by weak modulus enhancement i.e. hardness after implantation and annealing increased more significantly than the elastic modulus.

The results for hardness and elastic modulus for 50, 100, 150 nm print depths are presented in Tables 1 and 2, and the corresponding plot – in Fig. 2.

The initial sample hardness decreased a little with the print depth from 50 to 150 nm. This is common scale effect (indentation size effect). The hardness of implanted layer was higher a little, especially at 50 nm depth. Annealing after implantation resulted in a sharp increase of the surface layer hardness, and in comparison with the initial material the depth decrease of hardness occurred more intensively. This was an effect of non-hardened material situated lower. Investigation of VT-6 wear resistance in the cylinder friction over its surface after double implantation by W and Mo demonstrated the wear decrease almost by 15 for the first hundreds of friction cycles. Then the wear began to increase and after 700 cycles reached its initial level. The samples manufactured in the form of dumb-bells were investigated to determine the fatigue resistance within the statistic range 7–10 samples per dependence [9]. After implantation by W and Mo ions the samples demonstrated increase in the fatigue resistance by 25–30%, and after thermal annealing in vacuum at 550 °C for 2 h demonstrated increase to 60–70% of their initial value. The phase composition of the implanted sample VT-6 was the following: α-Ti, β-Ti, Al_3Ti, Al_2Ti (Fig. 3a)

After annealing of the implanted samples basic changes were related to Al_3Ti, in particular, a separated peak (111) Al_3Ti appeared in the diffraction pattern. The results taken in a small angle geometry (0.5° angle) demonstrate that in the region between (001) and (100) α-Ti the emission intensity increased, which seems to be conditioned by additional line (111) Al_3Ti (Fig. 3b). Fig. 4a,b shows the energy spectra RBS taken for the VT-6 samples after double implantation of Mo and W ions for two various fluences. In these spectra one can find Al, Ti, V, O, elements, as well as implanted Mo and W ions. Table 3 presents the results of element analysis for VT-6 irradiated with 2×10^{17} cm^{-2} fluence over the sample depth, which were taken using a standard program. As it can be seen in the table, the maximum W concentration reached about 4.44 at.%, its maximum occurring at 95.8 nm depth (for 2×10^{17} cm^{-2} fluence). Mo concentration amounted about 11.65 at.% with the maximum at 95.8 nm depth. Also V (~2.19 at.%), Ti (43.57 at.%), Al (9.52 at.%) were found. An oxygen peak (61 at.%) occurred at about 40.8 nm, When the fluence increased to 5×10^{17} cm^{-2}, the maximum W concentration reached 11 at.%, Mo concentration increased to 38 at.% (see Table 4).

Fig. 5a,b shows W and Mo ion profiles obtained from the RBS energy spectra after implantation with 2×10^{17} cm^{-2} fluence and subsequent thermal annealing at 550 °C for 2 h. The thermal annealing resulted in smearing of the profile, decreasing peak W and Mo concentration.

Calculation of efficient diffusion coefficients for the VT-6 samples on the basis of these profiles was made according to the formula

$$D_t = \frac{\sigma_i^2 - \sigma_t^2}{2t}, \tag{2}$$

where σ_i^2 is the width of peak W and Mo concentration at a half height at room temperature, σ_t^2 is the width of peak W, Mo concentration at a half height after annealing at 550 °C for 2 h, t is the annealing time, demonstrating that D_{Mo} was about

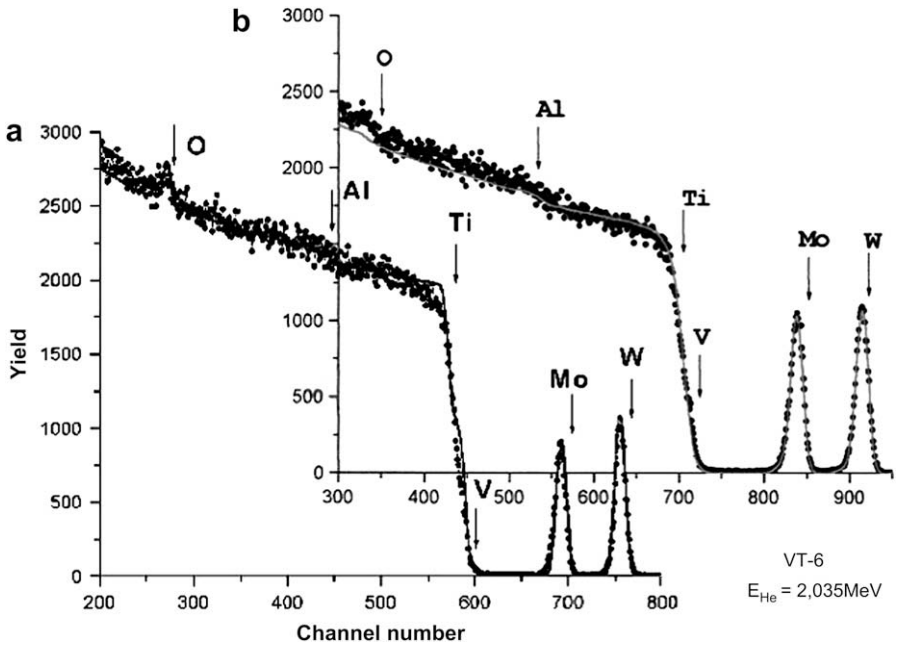

Fig. 4. Energy RBS spectra obtained for the VT-6 samples after double W and Mo ion implantation with 2×10^{17} cm^{-2} fluence (a) and with 5×10^{17} cm^{-2} fluence (b).

Table 3
Element concentration over VT-6 sample depth with 2×10^{17} cm^{-2} fluence.

Depth, nm	Elemental composition (at.%)					
	W	Mo	V	Ti	Al	O
408.4	.00	.00	2.17	26.44	9.70	61.69
958.4	4.44	11.11	2.19	43.53	9.57	29.16
2524.1	.00	.00	2.17	88.14	9.69	.00
4089.8	.00	.00	2.17	88.14	9.69	.00
160658.9	.00	.00	2.17	88.14	9.69	.00

Table 4
Element concentration over VT-6 sample depth with implantation fluence 5×10^{17} cm^{-2}.

Depth, nm	Elemental composition (at.%)							
	W	Mo	Fe	V	Ti	Al	O	C
85.2	11.06	.00	0.95	3.54	36.02	6.96	0.00	41.47
224.3	7.08	38.44	0.95	3.62	42.67	7.24	0.00	0.00
364.6	0.80	12.10	1.03	3.98	59.59	8.67	13.83	0.00
740.1	0.21	1.28	1.01	4.08	76.11	8.92	8.39	0.00
1483.9	0.10	1.05	1.00	4.03	79.90	8.88	5.04	0.00
156303.3	0.11	1.04	1.02	4.12	84.52	9.19	0.00	0.00

2.8×10^{-8} cm^2/s, and for tungsten ions – essentially lower and amounted D_W 10^{-9} cm^2/s.

Evidently, an increased concentration of radiation defects, as well as implantation of W and Mo impurities resulted in the increased hardness in the near surface layer (almost by 2). In our opinion, this also may be related to oxicarbide formation i.e. under W and Mo ion implantation into VT-6 with 2×10^{17} cm^{-2} fluence the maximum W concentration peak was 5 at.% and 11 at.% for Mo. At the same time, a fluence increase to 5×10^{17} cm^{-2} enhanced also the maximum W concentration to 12–14 at.%, and Mo reaching 38 at.%.

4. Conclusion

In this work it was demonstrated that the double implantation of Mo and W ions into titanium alloys VT-6 with 5×10^{17} cm^{-2} resulted in formation of concentration profiles with high element concentration at the maximum. Thermal annealing of VT-6 samples at 550 °C for 2 h resulted in the decreased peak Mo and W concentration and smearing of the element profiles.

Nanohardness measurements demonstrated that maximum hardness change was observed at about 50 nm depth, at 150 nm its

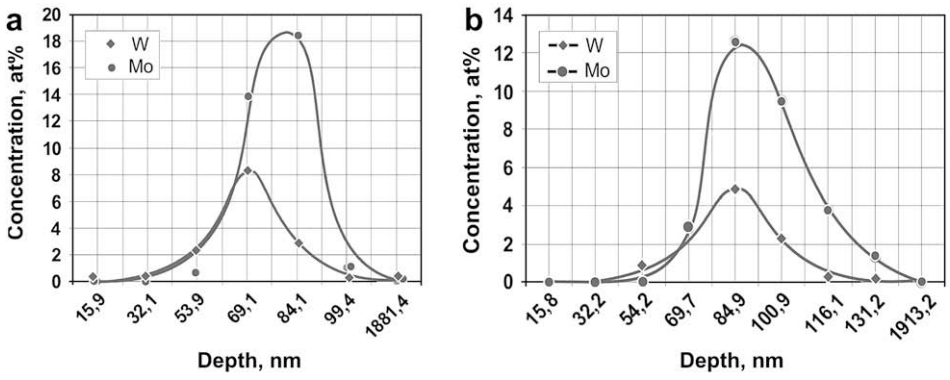

Fig. 5. Profiles of W and Mo ions obtained after implantation with 2×10^{17} cm^{-2} fluence (a) and subsequent thermal annealing in vacuum at 550 °C for 2 h (b).

value being essentially lower. After thermal annealing an elastic recovery of a print depth in unloading was a little higher than for the initial sample, which indicated that the hardness growth was accompanied by a weaker elastic modulus increase. After implantation and annealing the sample hardness reached higher values than the elastic modulus for the VT-6 samples.

Thermal annealing after Mo and W ion implantation resulted in a sharp hardness increase of a near surface layer. The hardness decrease with a depth was more significant in comparison with the initial samples, i.e. it seemed to be explained by influence of a lower layer (a non-hardened material).

A phase composition of VT-6 was also presented: α-Ti, β-Ti, Al_2Ti, Al_3Ti. All the changes occurring after annealing of the samples by two types of ions seem to be related to Al_3Ti phase (i.e. the fully separated peak (111) Al_3Ti). Simultaneously, in the region (001) and (100) α-Ti an increased emission intensity was observed, which was conditioned by an additional line (111) Al_3Ti.

W and Mo ion implantation with 5×10^{17} cm^{-2} fluence resulted in increased hardness – almost by 100% at 50 nm depth and its decrease at 150 nm.

References

[1] Hirvonen JK. Annu Rev Mater Sci 1989;19:401.
[2] Lavrentyev VI, Pogrebnjak AD, Sandrik P. JETP Lett 1997;65(8):651–3.
[3] Lavrentyev VI, Pogrebnjak AD. Surf Coat Technol 1998;99:24–32.
[4] Pogrebnjak AD, Kobzev AP, Gritsenko BP, Sokolov S, Bazyl E, Sviridenko N, et al. Jpn J Appl Phys 1999;38:L248–51.
[5] Pogrebnjak AD, Bazyl EA, Sviridenko NV. Prog Metal Phys 2004;5:257–81. Kiev.
[6] Pogrebnjak AD, Tolopa AM. Nucl Instrum Methods 1990;B52:24–43.
[7] Pogrebnjak Alexander, Kobzev Alexander, Gritsenko Boris P, Sokolov S, Bazyl E, Sviridenko N, et al. J Appl Phys 2000;87(5):2142.
[8] Pogrebnjak Alexander D, Bakharev OG, Pogrebnjak NA, Tsvintarnaya Yu.V, Shablya VT, Sandrik R, et al. Phys Lett 2000;A265:225–32.
[9] Pogrebnjak AD, Bazyl EA. Vacuum 2002;64:1–7.
[10] Komarov FF. Ion implantation on metals. M. Energoatomizdat; 1990. p. 260.
[11] Hirvonen JK. Ion Implantation into Metals. Moskow: Metallurgia; 1985. p. 457.
[12] Mandl S, Gerlach JW, Raushenbach B. Surf Coat Technol 2005;196:293–7.
[13] Kadyrzhanov KK, Komarov FF, Pogrebnjak AD, Rusakov VS, Turkebaev T. Ion beam and ion-plasma modification of materials. Moscow: Moscow State Univ.; 2005. p. 640.
[14] Azarenkov NA, Beresnev VM, Pogrebnjak AD. Structure and properties of coatings and modified layers of materials. Kharkov: Kharkov Nation. Univ.; 2007. p. 560.
[15] Oliver WC, Pharr GM. J Mater Res 1992;7(6):1564–83.